A Journal of the Gesellschaft Deutscher Chemiker

Angewandte International Edition

GDCh

Chemie

www.angewandte.org

Accepted Article

Title: Hydrophobic Metal Halide Perovskites for Visible-Light Photoredox C-C Bond Cleavage and Dehydrogenation Catalysis

Authors: Zonghan Hong, Wee Kiang Chong, Andrew Yun Ru Ng, Mingjie Li, Rakesh Ganguly, Tze Chien Sum, and Han Sen Soo

To be cited as: *Angew. Chem. Int. Ed.* 10.1002/anie.201812225
Angew. Chem. 10.1002/ange.201812225

Link to VoR: http://dx.doi.org/10.1002/anie.201812225
http://dx.doi.org/10.1002/ange.201812225

WILEY-VCH

10.1002/anie.201812225

WILEY-VCH

COMMUNICATION

Hydrophobic Metal Halide Perovskites for Visible-Light Photoredox C-C Bond Cleavage and Dehydrogenation Catalysis

Zonghan Hong,[a] Wee Kiang Chong, Andrew Yun Ru Ng,[a] Mingjie Li,[b] Rakesh Ganguly,[a] Tze Chien Sum,*[b] and Han Sen Soo*[a][c]

Abstract: Two-dimensional lead and tin halide perovskites were prepared by intercalating the long alkyl group 1-hexadecylammonium (HDA) between the inorganic layers. We observed visible-light absorption, narrow-band photoluminescence, and nanosecond photoexcited lifetimes in these perovskites. Due to their hydrophobicity and stability even in humid air, we applied these perovskites in the decarboxylation and dehydrogenation of indoline acids using $(HDA)_2PbI_4$ or $(HDA)_2SnI_4$ as photoredox catalysts, with quantitative conversions and high yields for the former. We highlight another original application of the metal halide perovskites.

Hybrid lead halide perovskites have received overwhelming attention over the past decade due to their exceptional performance as optoelectronic materials. Specifically, the methylammonium (MA), formadinium (FA), and cesium lead halide perovskites have been incorporated into solar cells that have achieved solar energy conversion efficiencies in excess of 22%.[1] Furthermore, $MAMX_3$, $FAMX_3$, $CsMX_3$ (M = Pb, Sn; X = I, Br, Cl), and their mixed ion permutations have found applications in light-emitting diodes,[2] non-linear absorption,[3] and lasers.[4] However, the use of these perovskites in photocatalysis and artificial photosynthesis have been limited,[5] despite their remarkable light harvesting abilities.

Photoredox catalysis has recently been established as a versatile methodology in the synthetic toolkit of organic chemists through a series of seminal studies by MacMillan,[6] Yoon,[7] Stephenson, and Fukuzumi,[8] which have demonstrated its general applicability under mild reaction conditions. Nonetheless, the photosensitizers employed in most photoredox reactions have predominantly been Ru- or Ir-based dyes that harvest radiation from the blue-end of the optical spectrum, due to their combination of effective photoexcited state lifetimes and suitable redox potentials for mediating the desired chemistry. In this regard, our team has been developing original aspects of the principal functions of an integrated artificial photosynthetic unit comprising exclusively earth-abundant elements, including visible light harvesters,[9] robust materials to facilitate charge separation,[10] and multielectron (photo)redox catalysis.[11] A particular challenge has been the discovery of heterogeneous photosensitizers that can span the visible spectrum and possesses suitable redox properties to mediate single electron transfer (SET) processes in photoredox reactions.[12]

The outstanding solar conversion efficiencies and widespread adoption of hybrid lead halide perovskites in optoelectronic devices lately suggest that they may be promising candidates as functional catalytic materials in photoredox chemistry. Nonetheless, some widely acknowledged shortcomings of the most popular $MAPbI_3$, $FAPbI_3$, and $CsPbI_3$ perovskites are their susceptibility to degradation under moist conditions and phase instability,[13] which has largely precluded their use in chemical reactions where solvents are involved. A number of recognized decomposition pathways include the deprotonation or leaching of the MA and FA cations, the unusually high iodide conductivity, and the inhomogeneous grain characteristics of perovskite layers, all of which turn perovskites into metastable materials.[14]

In this context, we sought hydrolytically stable, two-dimensional (2D), crystalline perovskites to circumvent their documented degradation deficiencies and create more robust materials suitable for driving photoredox reactions in organic solvents. Here, we present the preparation of structurally defined 2D perovskites containing hydrophobic hexadecylammonium (HDA) cations as the intercalating layers between the metal halide nanosheets to form $(HDA)_2MI_4$ (M = Pb, Sn). The Sn-based variant illustrates the viability of a comparatively less toxic lead-free perovskite for our application. A simple synthetic approach was developed and the materials were characterized rigorously. Variable temperature photoluminescence (VTPL) measurements confirm the radiative recombinations, and allude to their potential in enabling SET reactions in organic solvents. We have further exploited these new materials in photoredox decarboxylations and dehydrogenations to illustrate that these hydrophobic perovskites are viable as light harvesters for photodriven organic syntheses.

One of our motivations was to improve the stability of metal halide perovskites in solvents, especially protic media. We anticipated that long, hydrophobic, aliphatic chains close-packed in the perovskite structure between the inorganic layers would repel water molecules. Thus, we used the commercially available 1-hexadacylamine to prepare the corresponding ammonium iodide and the 2D metal halide perovskites. We used tetrahydrofuran (THF) for the crystallization and preparation of the perovskites due to the low energy cost of removing the volatile THF.

The successful synthesis of $(HDA)_2PbI_4$ and $(HDA)_2SnI_4$ was established by single crystal X-ray diffraction (XRD) studies

[a] Zonghan Hong, Andrew Y.R. Ng, Dr. Rakesh Ganguly, Dr. Han Sen Soo
Division of Chemistry and Biological Chemistry, School of Physical and Mathematical Sciences, Nanyang Technological University, 21 Nanyang Link, Singapore 637371, Singapore
E-mail: hansen@ntu.edu.sg
[b] Dr. Mingjie Li, Prof. Tze Chien Sum
Division of Physics and Applied Physics, School of Physical and Mathematical Sciences, Nanyang Technological University, 21 Nanyang Link, Singapore 637371, Singapore
E-mail: tzechien@ntu.edu.sg
[c] Dr. Han Sen Soo
Solar Fuels Laboratory, Nanyang Technological University, 50 Nanyang Avenue, Singapore 639798, Singapore
Supporting information for this article is given via a link at the end of the document. CCDC 1856670 ($(HDA)_2SnI_4$) and CCDC 1856671 ($(HDA)_2PbI_4$).

10.1002/anie.201812225

(Figure 1). Remarkably, the long C_{16} alkyl chains stack orderly to form a 2D layered structure up to micron scales based on the sizes of the single crystals obtained (Table S2). The $(PbI_6)^{4-}$ octahedron units remain mostly undistorted in the 2D inorganic layer. The overlap of the orbitals between Pb and I are expected to be effective, resulting in a distinct separation between the HOMOs and LUMOs, and hence a relatively larger band-gap. The phase purity was confirmed by powder X-ray diffraction (PXRD) experiments; no HDAI or PbI_2 precursors were observed in the diffraction data (Figure 1). The PXRD pattern of $(HDA)_2PbI_4$ matched reasonably with the simulated pattern based on the single crystal data, although there is preferred orientation of some Miller indices in the experimental sample. Compared to the Pb counterpart, $(HDA)_2SnI_4$ showed a shift of the PXRD peaks (e.g. for the (004) and (006) planes) toward higher angles due to the smaller *d*-spacing (Figure S2).

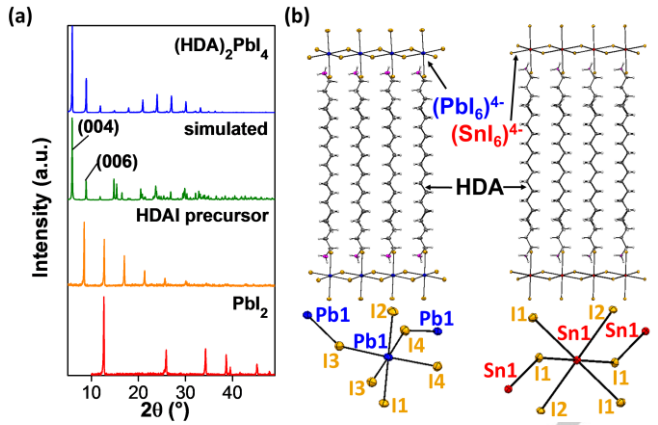

Figure 1. (a) PXRD patterns of $(HDA)_2PbI_4$ and its precursors. (b) Crystal structures of $(HDA)_2PbI_4$ and $(HDA)_2SnI_4$.

The elemental contents and purities of the perovskites were verified by X-ray photoelectron spectroscopy (XPS) and elemental analyses. The XPS data were consistent with Pb (Figure S3) and Sn (Figure S4) in the +2 oxidation state for the respective compounds. The IR spectra of the HDAI salt and the perovskites also clearly showed typical alkyl (C-H, 3000-2850 cm^{-1}) and amine (N-H, 3500-3100 cm^{-1}) stretches (Figure S5). The light absorbing abilities of the HDA based perovskites were probed by UV-visible diffuse reflectance spectroscopy (UV-vis DRS), as shown in Figure 2a. The absorption of $(HDA)_2PbI_4$ showed an onset at 520 nm and an exciton peak at 483 nm. $(HDA)_2SnI_4$ featured a wider range starting at 700 nm with multiple, unevenly spaced, broad and shallow absorption bands, most likely due to a Rydberg series of Wannier-Mott excitons.[15] Other contributions could include variations in the band gap caused by different I-Sn-I bond angles due to the flexible nature of the HDA chains and scattering effects from the polycrystalline sample, although these effects would not be fully consistent with the multiple, reproducible bands observed.[15] The band gaps are estimated to be 2.3 eV and 1.9 eV for $(HDA)_2PbI_4$ and $(HDA)_2SnI_4$ respectively, based on the Tauc plots calculated from the UV-vis DRS data (Figure 2b).

We subsequently tested the stability of these perovskites in humid air. $(HDA)_2PbI_4$ formed a suspension in water, with larger pieces of the material afloat on the surface. The PXRD pattern of the sample after stirring for 30 min in water was indistinguishable from the pristine $(HDA)_2PbI_4$ (Figure 2c). Contact angle (CA) measurements also confirmed the hydrophobicity with an average angle of 98.4° (Table S1, Figure S6). Most interestingly, $(HDA)_2PbI_4$ was still emissive when irradiated with UV while suspended in water, and the PL maximum was determined to be 500 nm (Figure 2d) after excitation at 350 nm. The modest Stokes shift is likely due to the high exciton binding energy that leads to less energy loss by carrier-phonon interactions, and is often observed in low dimensional perovskites.[16] However, $(HDA)_2SnI_4$ did not exhibit the same stability, likely due to the oxidation of Sn(II) to Sn(IV).

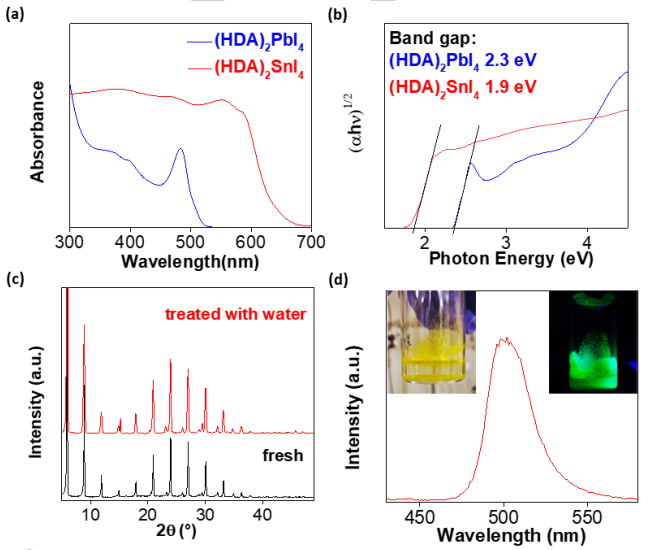

Figure 2. (a) UV-vis DRS spectra and (b) Tauc plots of the HDA Pb and Sn perovskites. (c) PXRD pattern of $(HDA)_2PbI_4$ before (black) and after (red) suspending in water (100 mg in 1 mL). (d) PL data from $(HDA)_2PbI_4$ suspended in water excited at 350 nm.

To further investigate the photophysical properties of $(HDA)_2PbI_4$, we conducted VTPL measurements down to 80 K.[17] As shown in Figure 3a, a significant blue shift was observed on cooling, which concurs with the expectation based on the Varshni equation on the temperature dependence of semiconductor bandgaps.[18] We also expect that the Pb-I bonds will contract at those low temperatures, resulting in a stronger interaction between overlapping orbitals, a higher Pb-I bond strength, and a wider energy gap between the valence and conduction bands. Time-resolved PL (TRPL) studies were also performed at variable temperatures. Figure 3b shows the PL decay transients from 80 to 300 K that could be consistently fitted bi-exponentially, revealing two decay processes, albeit with different weighting. The faster process (0.32 ± 0.01 to 0.17 ± 0.01 ns) likely originated from exciton recombination in the defect-rich region, while the slower process (3.0 ± 0.01 to 1.5 ± 0.01 ns) could arise from the intrinsic exciton recombination. The PL lifetime increased at lower temperatures suggesting the suppression of the thermal assisted non-radiative trapping by defects at higher temperatures (Figure S7). Critically, the slower processes are longer lived than diffusion control,[19] paving the way for charge transfer after photoexcitation. We also determined the valence band maximum (VBM) as 5.70

10.1002/anie.201812225

eV (Figure 3c) by photoelectron spectroscopy in air (PESA), which corresponded to a potential of 1.20 V vs NHE. Coupled with the high stability in organic media, our data suggested a potential application of $(HDA)_2PbI_4$ as a visible-light photosensitizer for oxidation reactions.

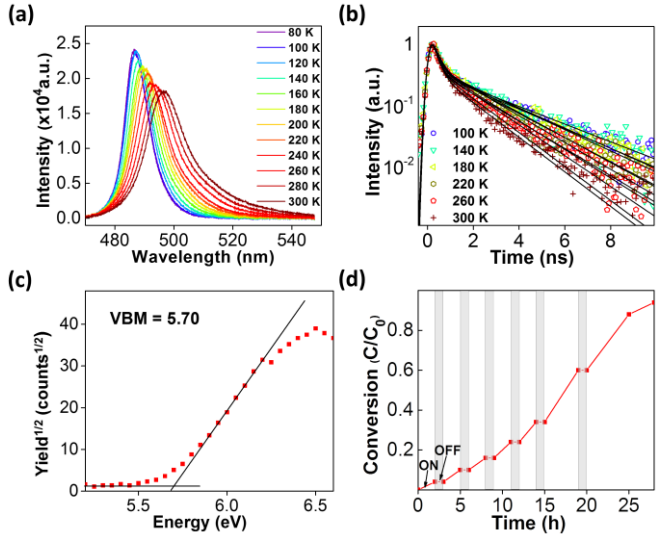

Figure 3. (a) VTPL and (b) VT-TRPL spectra of $(HDA)_2PbI_4$ after exciting at 390 nm. (c) PESA data of $(HDA)_2PbI_4$ with the intercept at the abscissa for the VBM. (d) "On-off" tests of the indoline-2-carboxylic acid decarboxylation.

Oxidation reactions with air are highly desirable due to increasing concern in the use of energy-intensive and stoichiometric oxidants. Among them, dehydrogenation and decarboxylation reactions are attractive for H_2 storage and C-C coupling synthesis respectively.[20] Moreover, carboxylic acids are ubiquitous in natural products and widely used as basic building blocks in synthesis.[21] Thus, photocatalytic oxidative decarboxylation presents a convenient approach to cleave a carbon-carbon bond to access valuable intermediates or products.[6b, 22] We found that indoline-2-carboxylic acid underwent decarboxylation to form indoline in the presence of $(HDA)_2PbI_4$ *under* N_2 and irradiation from a 48 W white LED lamp. On the other hand, both decarboxylation and dehydrogenation to indole occurred in the presence of O_2. Control experiments validated the necessity of $(HDA)_2PbI_4$ and visible light irradiation for the decarboxylation reaction (Table 1 entries 2-7). Although PbI_2 is known to be photoactive, the catalytic conversion for this reaction is negligible (entry 3). Both electron-deficient (Br and Cl substituted) and electron-rich substrates (methyl substituted) underwent decarboxylation to their corresponding indolines in high yields (entries 9-11, 13). Notably, no catalytically active homogeneous species was found from a filtration study to remove the insoluble perovskite (Figure S33). Moreover, most of the catalyst could be recovered by centrifugation and reused after a reaction, with only minor decomposition observed. SEM and AFM of the materials after catalysis suggested that the original polycrystalline samples had disintegrated into smaller nanocrystals (Figures S8 and S9). However, PXRD and XPS (Figures S10 and S11) indicated that the structure, elemental contents, and elements' oxidation states in the sample after catalysis remained mostly unchanged. The minor impurities, PbI_2 and HDAI, were catalytically inactive.

Table 1. Representative decarboxylation and dehydrogenation reactions catalyzed by the Pb and Sn 2D perovskites.

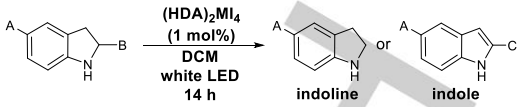

Entry	A	B	C	M	Condition variations	Yield (%) indoline	indole
1	H	COOH	-	Pb	-	98	-
2	H	COOH	-	-	with HDAI	14	-
3	H	COOH	-	-	with PbI_2	2	-
4	H	COOH	-	-	with I_2	0[a]	-
5	H	COOH	-	Pb	no light	1	-
6	H	COOH	-	-	no cat.	4	-
7	H	COOH	H	Pb	40 °C[b]	0	0
8	H	COOH	H	Pb	O_2	-	78
9	Br	COOH	-	Pb	-	81	-
10	Br	COOH	H	Pb	O_2		84
11	Cl	COOH	-	Pb	-	81	-
12	Cl	COOH	H	Pb	O_2	-	20
13	Me	COOH	-	Pb	-	83	-
14	Me	COOH	-	Sn	-	30	-
15	Me	COOH	H	Pb	O_2	-	<10
16	CF_3	H	H	Pb	O_2	-	48
17	H	Me	Me	Pb	O_2	-	17
18	H	Me	Me	Pb	DE, O_2	-	71
19	H	Me	Me	Sn	DE, O_2	-	47

[a]11% conversion to unknown product. [b]Up to the boiling point of DCM.

Furthermore, 5-trifluoromethylindoline and 2-methyl-indoline were evaluated as substrates for dehydrogenation, yielding 48% and 17% of the respective indoles (entries 16, 17). By using diethyl ether (DE) as a solvent, the yield of 2-methylindole could be raised to 71% (entry 18). We also explored photocatalysis by the lead-free $(HDA)_2SnI_4$ congener, but the decarboxylation of 5-methylindoline acid yielded 30% of the indoline (entry 14), while the dehydrogenation of 2-methyl-indoline led to a 47% yield of the indole in DE (entry 19). These moderate yields are likely due to the oxidative instability and abundance of traps for Sn(II) perovskites. Guided by previous reports on photoredox catalysis,[21, 23] we propose the mechanisms shown in Scheme 1.

Scheme 1. Proposed mechanisms for the decarboxylation (left) and dehydrogenation (right) reactions. [P] represents the perovskites.

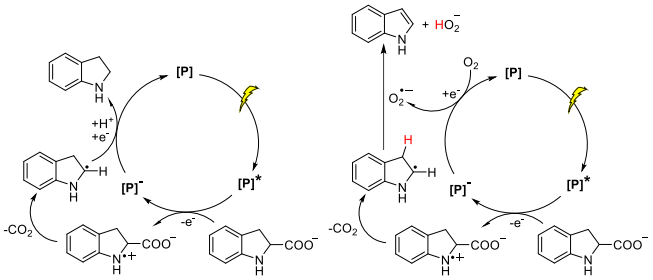

We first applied ferrocene as a hole scavenger and observed that it impeded the decarboxylation reaction. On the other hand, when $AgBF_4$ was used as an electron scavenger, it behaved as a sacrificial electron acceptor and did not hinder the catalysis, indicating that the rate determining step was likely to be

photooxidation by our catalysts. We also observed that the yield dropped to 32% for dehydrogenation in the presence of excess Tiron (disodium 4,5-dihydroxy-1,3-benzenedisulfonate-4,5-dihydroxy-1,3-benzenedisulfonate) as a superoxide scavenger[24] which verified the role of superoxide radicals for the proposed dehydrogenation mechanism (Figures S34-36). An "on-off" irradiation study (Figure 3d) excluded a radical chain mechanism.

In summary, we have synthesized 2D metal halide perovskites by intercalating HDA between the inorganic layers. Detailed characterization of these new perovskites highlighted valuable features for photoredox catalysis. Notably, their stability in organic solvents, even in the presence of water, provided an opportunity to use them for organic synthesis. As a conceptual demonstration, $(HDA)_2PbI_4$ and $(HDA)_2SnI_4$ effected the photocatalytic redox-neutral decarboxylation and oxidative dehydrogenation of indoline carboxylic acids. This report showcases another original application for halide perovskites, and illustrates their use in photoredox organic synthesis.

Acknowledgements

H.S.S. is supported by MOE Tier 1 grants RG 12/16 and RG 13/17 and an A*STAR AME IRG grant A1783c0002. We also thank the Solar Fuels Lab at NTU. T.C.S. acknowledges funding from MOE (Tier 1 grant RG 173/16 and Tier 2 grants MOE2015-T2-2-015 and MOE2016-T2-1-034). T.C.S. and M.L. are also funded by the Singapore NRF via the Competitive Research Programme NRF-CRP14-2014-03 and the NRF Investigatorship Programme NRF-NRFI-2018-04. We thank Prof. Xing Yi Ling and Mr. Ya-Chuan Kao for help with contact angle experiments.

Keywords: 2D metal halide perovskites • decarboxylation • hydrophobic perovskite • photocatalysis • photooxidation

[1] a) J. P. Correa-Baena, M. Saliba, T. Buonassisi, M. Gratzel, A. Abate, W. Tress, A. Hagfeldt, *Science* **2017**, *358*, 739-744; b) Q. Lin, A. Armin, P. L. Burn, P. Meredith, *Acc. Chem. Res.* **2016**, *49*, 545-553; c) D. P. McMeekin, et al., *Science* **2016**, *351*, 151-155; d) W. S. Yang, et al., *Science* **2017**, *356*, 1376-1379; e) G. Xing, N. Mathews, S. Sun, S. S. Lim, Y. M. Lam, M. Gratzel, S. Mhaisalkar, T. C. Sum, *Science* **2013**, *342*, 344-347.

[2] a) E. R. Dohner, A. Jaffe, L. R. Bradshaw, H. I. Karunadasa, *J. Am. Chem. Soc.* **2014**, *136*, 13154-13157; b) Z. K. Tan, et al., *Nat. Nanotechnol.* **2014**, *9*, 687-692.

[3] a) Y. Wang, X. M. Li, X. Zhao, L. Xiao, H. B. Zeng, H. D. Sun, *Nano Lett.* **2016**, *16*, 448-453; b) R. Zhang, J. D. Fan, X. Zhang, H. H. Yu, H. J. Zhang, Y. H. Mai, T. X. Xu, J. Y. Wang, H. J. Snaith, *ACS Photonics* **2016**, *3*, 371-377.

[4] a) G. Xing, N. Mathews, S. S. Lim, N. Yantara, X. Liu, D. Sabba, M. Grätzel, S. Mhaisalkar, T. C. Sum, *Nat. Mater.* **2014**, *13*, 476-480; b) H. M. Zhu, et al., *Nat. Mater.* **2015**, *14*, 636-642.

[5] a) S. Park, W. J. Chang, C. W. Lee, S. Park, H.-Y. Ahn, K. T. Nam, *Nat. Energy* **2016**, *2*, 16185; b) Y. F. Xu, M. Z. Yang, B. X. Chen, X. D. Wang, H. Y. Chen, D. B. Kuang, C. Y. Su, *J. Am. Chem. Soc.* **2017**, *139*, 5660-5663; c) L. Wang, H. Xiao, T. Cheng, Y. Li, W. A. Goddard, 3rd, *J. Am. Chem. Soc.* **2018**, *140*, 1994-1997.

[6] a) C. Le, T. Q. Chen, T. Liang, P. Zhang, D. W. C. MacMillan, *Science* **2018**, *360*, 1010-1014; b) Y. Liang, X. Zhang, D. W. C. MacMillan, *Nature* **2018**, *559*, 83-88; c) D. A. Nicewicz, D. W. MacMillan, *Science* **2008**, *322*, 77-80.

[7] a) T. R. Blum, Z. D. Miller, D. M. Bates, I. A. Guzei, T. P. Yoon, *Science* **2016**, *354*, 1391-1395; b) M. A. Ischay, M. E. Anzovino, J. Du, T. P. Yoon, *J. Am. Chem. Soc.* **2008**, *130*, 12886-12887.

[8] a) S. Fukuzumi, K. Ohkubo, *Chem. Sci.* **2013**, *4*, 561-574; b) J. M. Narayanam, J. W. Tucker, C. R. Stephenson, *J. Am. Chem. Soc.* **2009**, *131*, 8756-8757.

[9] a) K. Hasan, J. Y. Wang, A. K. Pal, C. Hierlinger, V. Guerchais, H. S. Soo, F. Garcia, E. Zysman-Colman, *Sci. Rep.* **2017**, *7*, 15520; b) J. W. Kee, Y. Y. Ng, S. A. Kulkarni, S. K. Muduli, K. Xu, R. Ganguly, Y. Lu, H. Hirao, H. S. Soo, *Inorg. Chem. Front.* **2016**, *3*, 651-662; c) M. Dokic, H. S. Soo, *Chem. Commun.* **2018**, *54*, 6554-6572.

[10] Y. C. Gong, D. P. Wang, R. B. Wu, S. Gazi, H. S. Soo, T. Sritharan, Z. Chen, *Dalton Trans.* **2017**, *46*, 4994-5002.

[11] a) S. Gazi, M. Dokic, A. M. P. Moeljadi, R. Ganguly, H. Hirao, H. S. Soo, *ACS Catal.* **2017**, *7*, 4682-4691; b) S. Gazi, W. K. H. Ng, R. Ganguly, A. M. P. Moeljadi, H. Hirao, H. S. Soo, *Chem. Sci.* **2015**, *6*, 7130-7142; c) H. Y. Shao, S. K. Muduli, P. D. Tran, H. Sen Soo, *Chem. Commun.* **2016**, *52*, 2948-2951; d) J. H. Lim, X. Engelmann, S. Corby, R. Ganguly, K. Ray, H. S. Soo, *Chem. Sci.* **2018**, *9*, 3992-4002; e) D. Ghosh, B. Febriansyah, D. Gupta, L. K. S. Ng, S. B. Xu, Y. H. Du, T. Baikie, Z. L. Dong, H. S. Soo, *ACS Nano* **2018**, *12*, 5903-5912.

[12] a) S. Lian, M. S. Kodaimati, D. S. Dolzhnikov, R. Calzada, E. A. Weiss, *J. Am. Chem. Soc.* **2017**, *139*, 8931-8938; b) Z. Zhang, K. Edme, S. Lian, E. A. Weiss, *J. Am. Chem. Soc.* **2017**, *139*, 4246-4249; c) S. Lian, M. S. Kodaimati, E. A. Weiss, *ACS Nano* **2018**, *12*, 568-575.

[13] a) A. M. A. Leguy, et al., *Chem. Mater.* **2015**, *27*, 3397-3407; b) B. R. Vincent, K. N. Robertson, T. S. Cameron, O. Knop, *Can. J. Chem.* **1987**, *65*, 1042-1046; c) J. L. Yang, B. D. Siempelkamp, D. Y. Liu, T. L. Kelly, *ACS Nano* **2015**, *9*, 1955-1963.

[14] T. M. Koh, K. Thirumal, H. S. Soo, N. Mathews, *ChemSusChem* **2016**, *9*, 2541-2558.

[15] a) J. C. Blancon, et al., *Nat. Commun.* **2018**, *9*, 2254; b) K. Wang, C. Wu, D. Yang, Y. Jiang, S. Priya, *ACS Nano* **2018**, *12*, 4919-4929; c) D. B. Mitzi, C. D. Dimitrakopoulos, L. L. Kosbar, *Chem. Mater.* **2001**, *13*, 3728-3740.

[16] C. M. Iaru, J. J. Geuchies, P. M. Koenraad, D. Vanmaekelbergh, A. Y. Silov, *ACS Nano* **2017**, *11*, 11024-11030.

[17] a) L. Lanzetta, J. M. Marin-Beloqui, I. Sanchez-Molina, D. Ding, S. A. Haque, *ACS Energy Lett.* **2017**, *2*, 1662-1668; b) M. I. Saidaminov, et al., *ACS Energy Lett.* **2016**, *1*, 840-845; c) S. J. Yoon, K. G. Stamplecoskie, P. V. Kamat, *J. Phys. Chem. Lett.* **2016**, *7*, 1368-1373.

[18] Y. P. Varshni, *Physica* **1967**, *34*, 149-154.

[19] a) H. Mayr, B. Kempf, A. R. Ofial, *Acc. Chem. Res.* **2003**, *36*, 66-77; b) S. H. Koenig, T. D. B. III, *Proc. Nat. Acad. Sci. USA* **1972**, *69*, 2422-2425.

[20] C. Gunanathan, D. Milstein, *Science* **2013**, *341*, 1229712-1229723.

[21] C. P. Johnston, R. T. Smith, S. Allmendinger, D. W. C. MacMillan, *Nature* **2016**, *536*, 322-325.

[22] C. K. Prier, D. A. Rankic, D. W. C. MacMillan, *Chem. Rev.* **2013**, *113*, 5322-5363.

[23] M. Zheng, J. Shi, T. Yuan, X. Wang, *Angew. Chem. Int. Ed.* **2018**, *57*, 5487-5491.

[24] E. Hideg, C. Spetea, I. Vass, *Photosynth. Res.* **1995**, *46*, 399-407.

10.1002/anie.201812225

WILEY-VCH

Entry for the Table of Contents

COMMUNICATION

Hydrophobic perovskites for photocatalysis: Hydrophobic 2D Pb and Sn halide perovskites were synthesized under ambient conditions from solution-based methods and show contact angles over 90º, as well as dispersibility and photoluminescence in water, highlighting the hydrophobic behavior. The perovskites are also effective photocatalysts for visible-light driven redox-neutral decarboxylation and oxidative dehydrogenation reactions.

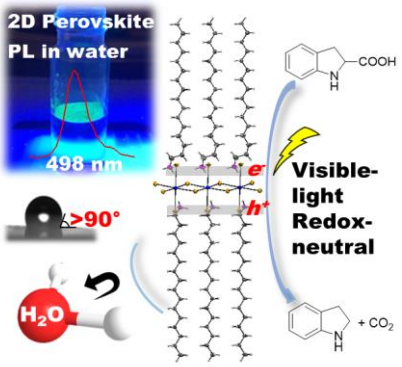

Zonghan Hong, Wee Kiang Chong, Andrew Yun Ru Ng, Mingjie Li, Rakesh Ganguly, Tze Chien Sum, and Han Sen Soo**

Page No. – Page No.

Hydrophobic Metal Halide Perovskites for Visible-Light Photoredox C-C Bond Cleavage and Dehydrogenation Catalysis